MEASUREMENT SCIENCE REVIEW, **17**, (2017), No. 3, 145-152

DE GRUYTER OPEN

MEASUREMENT SCIENCE REVIEW

Journal homepage: http://www.degruyter.com/view/j/msr

ISSN 1335-8871

Magnetic Resonance Super-resolution Imaging Measurement with Dictionary-optimized Sparse Learning

Jun-Bao Li[1], Jing Liu[2], Jeng-Shyang Pan[3], Hongxun Yao[4]

[1]*Department of Automatic Test and Control, Harbin Institute of Technology, Harbin 150080, China*
[2]*College of Information and Communication Engineering, Harbin Engineering University, Harbin 150001, China*
[3]*Fujian Provincial Key Lab of Big Data Mining and Applications, Fujian University of Technology, Fuzhou 350108, China*
[4]*School of Computer Science and Technology, Harbin Institute of Technology, Harbin 150001, China*

Magnetic Resonance Super-resolution Imaging Measurement (MRIM) is an effective way of measuring materials. MRIM has wide applications in physics, chemistry, biology, geology, medical and material science, especially in medical diagnosis. It is feasible to improve the resolution of MR imaging through increasing radiation intensity, but the high radiation intensity and the longtime of magnetic field harm the human body. Thus, in the practical applications the resolution of hardware imaging reaches the limitation of resolution. Software-based super-resolution technology is effective to improve the resolution of image. This work proposes a framework of dictionary-optimized sparse learning based MR super-resolution method. The framework is to solve the problem of sample selection for dictionary learning of sparse reconstruction. The textural complexity-based image quality representation is proposed to choose the optimal samples for dictionary learning. Comprehensive experiments show that the dictionary-optimized sparse learning improves the performance of sparse representation.

Keywords: Magnetic resonance imaging measurement, sparse learning, dictionary learning, super-resolution imaging.

1. INTRODUCTION

Magnetic Resonance Super-resolution Imaging Measurement (MRIM) is widely used in physics, chemistry, biology, geology, medical and material science, and especially in medical diagnosis. In the medical disease diagnosis, Magnetic Resonance Imaging (MRI) can image the organs and structures of body for clinical diagnosis. It performs better than X-ray, ultrasound, or computed tomography (CT) in the diagnosis of tumors, bleeding, or blood vessel diseases. MRI plays gradually a more important role in the diagnosis of various diseases. The current method is to improve the resolution through increasing free water magnetization of human tissue and organs. Accordingly, the method of increasing radiation time and radiation intensity of electromagnetic waves is widely applied to MR instruments. But the human body can be excessively heated by radiation which inactivates proteins. So, the hardware super-resolution imaging technology has its limitations on the practical clinical application. MRI can obtain the high-resolution image for the clinical diagnosis, but is limited by SNR, hardware, imaging time, and so on. Many methods are proposed to reconstruct the high-resolution image through signal processing and other machine learning methods. Sparse representation-based super-resolution reconstruction is a recently proposed method for image recovery. The sparse representation model-based image processing performs well on image denoising [1], image deblurring [2], [3], image restoration [4]. The sparse representation methods include rapid sparse representation [5], dictionary-based learning method, for example KSVD [6], MOD [7], pixel selection-based sparse representation [8], locality constrained sparse representation [9], precise dictionary representation [10], dictionary selection-based sparse representation [11]. Sparse representation methods are applied in many image processing techniques, including object detection via hyper spectral image [12], image fusion and restoration [13], and other image restoration [14], [15], image classification [16], and SR-based image classification and face recognition [17] techniques. In the previous works, image sparse super-resolution technologies were widely applied to medical image super-resolution, remote hyperspectral imaging, video and image super-resolution. The features of edge, texture, and structure are applied to image super-resolution [18]. For the dictionary training problem, the constraint dictionary method is proposed to SR-based image super-resolution [19], and the sparse domain based image deblurring is to solve the high-resolution image [20]. For SR-based medical image analysis, only a few SR-based medical image analysis methods were proposed in previous works, for example,

DOI: 10.1515/msr-2017-0018

sparse representation based MR spectroscopy quantification [21], constrained generative regression model-based fMRI analysis [21], filter-base machine intelligence [22]-[24], sparse coding based super-resolution learning [25], similar based image blocks sparse relations [26].

Based on the survey of the recent works on sparse reconstruction technologies, there are many researches on dictionary training, sparse parameters solution, sparse reconstruction. But to dictionary-optimized learning, less attention was paid in the previous works. They applied the traditional methods to training the dictionary with enough training samples. However, in many practical applications, i.e., MR, only limited samples are used to train the dictionary. MR images have to be used to train the dictionary for the excellent performances of super-resolution. How to sufficiently use the definite MR samples is a crucial issue of improving the MR super-resolution. The performance of dictionary learning training directly affects the quality of the image reconstruction. Thus, how to optimize the training procedure is a crucial problem. We have to select optimal samples to ensure the effectiveness of training dictionary blocks. In this paper, we present a framework of dictionary training method based on optimizing the samples from the limited MR training samples. Texture-complexity based optimization is to choose the training samples from the training samples. The texture complexity is measured with the gray-consistency method. Based on this dictionary training method, we propose a framework of dictionary training samples-optimized sparse reconstruction-based super-resolution MR imaging.

2. FRAMEWORK AND ALGORITHM

A. Framework

The framework is shown in Fig.1. In this framework, the coupled dictionaries are trained with sample selection via the image quality representation based on the gray-consistency method. The MR image training samples are selected for training the high-low MR image blocks from the training image samples, and these training samples are simultaneously trained low-high resolutions of dictionaries. The framework applies the machine learning-based dictionary block learning. In the definite scale of high resolution images, the optimized chosen high resolution images are spliced into multiple image blocks to train the high-resolution dictionary. Accordingly, the low-resolution dictionary is trained by the low image down-sampled high resolution image. In the same way, the multiple image blocks are achieved through splicing the low resolution training images. Under the SR-based super-resolution construction framework, the SR coefficients are solved with sparse representation constrained optimization equation, accordingly, the image can be represented by the combinations of the image block from the dictionary under the SR parameters. On the SR construction, the high resolution of image is computed under the sparse coefficients and the high-resolution dictionary.

As shown in the framework, the crucial issue is to choose the optimized training samples for dictionary training. For the SR construction-based MR super-resolution, dictionary training often depends on a large number of training samples, but in the practical applications we can obtain a sufficient number of training samples, in other words, among the definite number of training samples some training samples are not effective for dictionary training, so that the dictionary is not ideal for sparse representation of image. In the framework, the crucial step is the training sample selection, and the complexity-based image quality representation is presented for MR image sample selection for training the high-low MR image blocks. If the texture complexity of MR training images is higher, then the quality of super-resolution is better. Not all MR images are effective for the dictionary training. We apply the gray consistent-based complexity measuring method to discriminately classify the MR image sample. On the basis of discriminant MR training sample, the optimal training images are selected for the training dictionary, the samples that are not fitted to the dictionary training of MR images are deleted, which improve the training performance of dictionary.

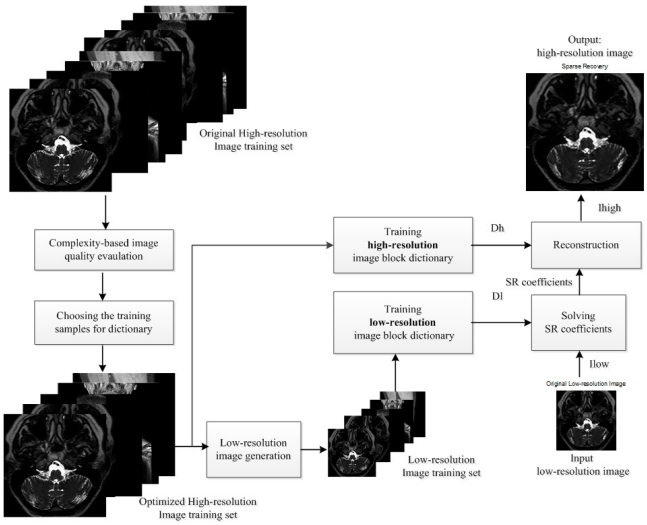

Fig.1. Framework of Dictionary Training Samples-Optimized Sparse Reconstruction-Based Super-resolution MR Imaging.

B. Algorithm

Firstly, we describe the algorithm of the sample selection for dictionary training. In this algorithm, the complexity of MR image depends on the type of object and representation method. The description of image complexity is based on the angle of the whole, the angle of the region and the angle of the target. So, the spatial distribution of gray level is unique to the image, and the two-dimensional image will not be related to the spatial location. The gray distribution reflects the spatial distribution of the image, which describes the size and the spatial distribution of the gray patches. The distribution of gray space is used to describe the image correlation and symmetry. The features include concentrated

or dispersed gray consistency, the existence of repetition, symmetry and so on. The consistency of gray level is used to describe the complexity of the image as follows

$$U = \sum_{a=2}^{m-1}\sum_{b=2}^{n-1}(f(a,b)-\bar{f})^2 \tag{1}$$

$$\bar{f} = \frac{1}{8}\left(\sum_{i=-1}^{1}\sum_{j=-1}^{1} f(a+i,b+j) - f(a,b)\right) \tag{2}$$

where $f(a,b)$ is the pixel value in the position, $\bar{f}$ is the mean value of 8 pixels round the center. Gray consistency shows the difference of each pixel and the pixel gray value accumulation. The greater is the difference in description of the image pixel gray value wind speed change, the more complex is the performance of the different image texture. We implement some experiments on the performance of the gray consistency method.

The algorithm procedure is shown in Table 1. If the image samples based on texture complexity, or most of the regional images as the invalid area that is adjacent to the pixel point gradient value are selected, the human eye cannot distinguish between the image patches. So randomly selected is invalid area. Based on texture fuzzy region, more samples improve the performance of super-resolution reconstruction. Therefore, not all training samples are necessary for dictionary training, and only the training image sample with the complex textures can provide enough features of the image blocks for the dictionary training for SR.

Table 1. Algorithm procedure of training images selection.

Step 1. Compute the largest gradient and complexity of the training sample.
For the input image I_i, compute the first order and second order $f(I_i)$:

$$\begin{cases} f_1 = [-1,0,1], & f_2 = f_1^T \\ f_3 = [1,0,-2,0,1], & f_4 = f_3^T \end{cases}$$

Compute the complexity of all images I_i:

$$y_i = \sum_{a=2}^{m-1}\sum_{b=2}^{n-1}(I_i(a,b)-\bar{I}_i)^2, \quad \bar{I}_i = \frac{1}{8}\left(\sum_{i=-1}^{1}\sum_{j=-1}^{1} I_i(a+i,b+j) - I_i(a,b)\right)$$

where m and n are the number of row and column, and $I_i(a,b)$ is the pixel gray value of the point (a,b).
Step 2. Select the center line of two coordinates as the baseline.
Step 3. Project the center of each class to the baseline, and cluster the image data to the center of each class.
Step 4. Select the sample of the farthest distance from the center as the training sample.

Secondly, the algorithm of dictionary-learning super-resolution method is described as follows. The high-resolution image block dictionary D_h and the low-resolution image block dictionary D_l are trained by high-resolution and low-resolution of MR images. As the definition of SR method, the high-resolution I_{high} contains many image blocks B_{high}, which is represented as a sparse linear combination of the D_h and sparse representation parameter vector α as

$$B_{high} \approx D_h\alpha \tag{3}$$

The α is to recover B_{low} from the low-resolution MR image I_{low} according to the low and high resolution of D_l and D_h with the following optimization equations as follows.

$$\min \|a\|_1 \quad s.t. \|FD_l a - FB_{low}\|_2^2 \le \varepsilon \tag{4}$$

where F denotes the feature extractor for dictionary generation, which provides the constraint of similarity of the coefficients a and B_{low}. F improves the high prediction accuracy through computing coefficients. The high-pass filter is to extract the features because of the sensitivity of human vision. The high-frequency components of low-resolution image are to predict the high-frequency parts of high-resolution of MR image. Then the optimization equation (5) is transferred to the Lagrange problem:

$$\min_a \|FD_l a - FB_{low}\|_2^2 + \lambda\|a\|_1 \tag{5}$$

where λ is balance sparsity of B_{low}., and λ determines the construction performance. The super-resolution reconstruction $D_h\alpha$ of B_{low} is calculated adjacent B_{high}, so

$$\min \|a\|_1 \quad s.t. \|FD_l a - FB_{low}\|_2^2 \le \varepsilon_1 and \|MD_l a - m\|_2^2 \le \varepsilon_2 \tag{6}$$

where M extracts the overlapped region between the target block and previously reconstructed MR image. Supposed

$\overline{D} = \begin{bmatrix} FD_l \\ \beta MD_h \end{bmatrix}$, $\overline{B}_{low} = \begin{bmatrix} FB_{low} \\ \beta m \end{bmatrix}$, then

$$\min_a \|\overline{D}a - \overline{B}_{low}\|_2^2 + \lambda\|a\|_1 \tag{7}$$

The high-resolution block B_{high} is reconstructed with the optimal solution α^* of optimization equation (5) as follows.

$$B_{high} = D_h a^* \tag{8}$$

For the noised image, $I_{orginal}$ may not satisfy the reconstruction constraint of sparse representation-based construction. Under the blurring operator F_B and down-sampling operator F_S, I_{low} is achieved by high-resolution I_{high} as follows.

$$I^* = \arg\min_I \|F_S F_B I - I_{low}\|_2^2 + c\|I - I_{original}\|_2^2 \tag{9}$$

We applied gradient descent method to solve the constraint optimization equation based on the iteration method as

$$I(n+1) = I(n) + \eta[F_B^T F_S^T (I_{low} - F_S F_B I(n)) + c(I(n) - I_{original})] \tag{10}$$

where $I(n)$ is nth iteration of high-resolution MR image under the gradient step η. Finally, the solution I^* is the high-resolution reconstructed image of MR image $I_{orginal}$. So, the high-resolution of MR image I^* is reconstructed by α^* under the representations-based reconstructed constrained equation as

$$I^* = \arg\min_{I,\{a_{ij}\}} \left\{ \left\| F_S F_B I - I_{low} \right\|_2^2 + \lambda \sum_{i,j} \left\| a_{ij} \right\|_0 + \gamma \sum_{i,j} \left\| D_h a_{ij} - P_{ij} I \right\|_2^2 + \tau \rho(I) \right\} \quad (11)$$

Under the sparse representation coefficients α_{ij} in the (i,j) patch of I, and a penalty function $\rho(I)$ of encoding additional prior knowledge on the high-resolution and low resolution MR image.

3. RESULTS

In this section, we implement some experiments to testify the feasibility of the algorithm, and have the comprehensive evaluation of the performance of the algorithm. We apply real medical MR images. Some examples are shown in Fig.2. The images include brain, ankle, aorta, carotid artery, knee, neck, and foot. The size of the training dictionary is 125×512, and 512 feature blocks, 5×5 of image blocks, and overlap block is 4, balance parameter λ=0.1, and super-resolution rate is 1:2 and 1:4. The PSNR is to measure the super-resolution performance. In the feasibility of the dictionary training, in order to analyze each dictionary, we randomly choose a few of the training samples for dictionary training, and 1, 2, 3, 5, 10, 20, 105, 360 of MR images are chosen randomly to construct the training dictionary sets. In the performance evaluation, we repeated the experiments with the Monte-Carlo simulation method.

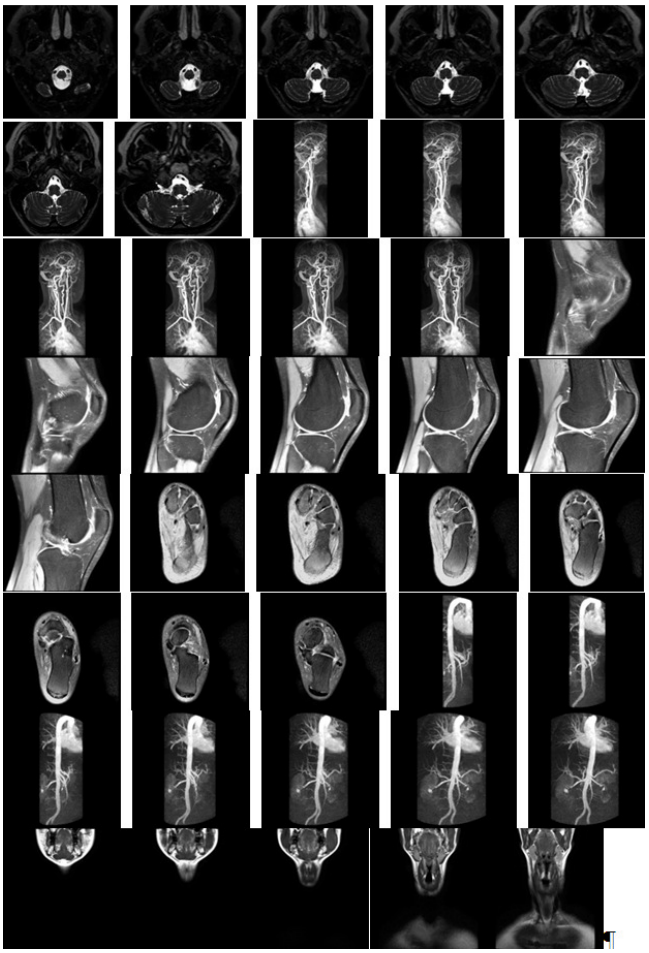

Fig.2. Examples of MRI sequence.

Table 2. Performance on MR super-resolution under the different training number.

	The number of training samples	**Dictionary**	**brain**	**ankle**	**aorta**	**carotid artery**	**knee**	**neck**	**foot**
1:2 of super-resolution	1	D1	31.77	28.71	35.70	31.72	30.51	30.19	30.42
	2	D2	32.15	28.80	35.97	31.97	30.58	30.25	30.74
	3	D3	32.31	28.84	36.05	32.07	30.60	30.31	30.87
	5	D4	32.25	28.85	36.05	32.02	30.59	30.33	30.78
	10	D5	32.28	28.88	36.05	32.04	30.57	30.33	30.79
	20	D6	32.27	28.87	36.02	32.05	30.59	30.33	30.79
	105	D7	32.31	28.87	36.05	32.04	30.58	30.36	30.81
	360	D8	32.21	28.86	35.98	32.00	30.56	30.29	30.71
1:4 of super-resolution	1	D9	29.39	25.20	32.71	29.00	27.08	27.46	27.88
	2	D10	30.05	25.41	32.96	29.23	27.11	27.54	28.23
	3	D11	29.63	25.33	32.84	29.13	27.10	27.53	28.19
	5	D12	29.83	25.39	32.90	29.20	27.09	27.56	28.20
	10	D13	29.92	25.44	32.99	29.28	27.12	27.62	28.28
	20	D14	29.86	25.38	32.94	29.26	27.11	27.59	28.27
	105	D15	29.84	25.40	32.97	29.25	27.10	27.61	28.22
	360	D16	29.95	25.42	32.98	29.34	27.14	27.67	28.26

A. On the dictionary optimization

In this section, we evaluate the dictionary generation based on optimizing the training samples for SR-based construction of MR image.

Secondly, 20 images from different classes are selected as training samples of dictionary generation, and a dictionary is trained by each image to generate 20 dictionaries for SR-based MR super-resolution image. In the experiments, the procedural parameters include that the size of training dictionary is 125×512, the characteristic of block is 512, the image block size is 5×5, the number of overlapped block is 4, the balance parameter is 0.1, and the rate of super-resolution is 1:2. Table 3. shows the performance of MR super-resolution under the different number of training samples for dictionary generation. The first column is the training image ID, the second is the dictionary ID, and the remaining columns are the PSNR performance under the different MR images. For each test image, the trend of PSNR changing corresponding to the number of training image is the same. The experiments show that the different training sample sets for dictionary generation affect the performance of SR-based construction, from the fact that the trend of PSNR corresponding to the 7 sets of test images is the same.

Thirdly, further analysis on the relationships between complexity of training images and reconstruction performance is shown in Table 4. The circle in the figure indicates that the PSNR is higher. The complexity of the dictionary is higher, better performance of image super-resolution reconstruction is achieved.

Table 3. Performance on the different number of training samples for dictionary learning (1:4 of MR super-resolution).

Image ID	Generated dictionary	brain	ankle	aorta	carotid artery	knee	neck	foot
1	D30	30.31	27.86	34.68	30.85	30.19	29.61	29.49
2	D31	31.95	28.57	35.69	31.78	30.40	29.98	30.49
3	D32	32.43	28.93	36.17	32.15	30.63	30.44	31.05
4	D33	32.14	28.79	35.98	31.93	30.60	30.37	30.81
5	D34	31.88	28.53	35.58	31.69	30.38	29.92	30.46
6	D35	32.23	28.83	36.04	32.02	30.61	30.31	30.79
7	D36	32.39	28.74	36.03	31.95	30.56	30.31	30.84
8	D37	30.47	27.94	34.80	30.98	30.21	29.69	29.74
9	D38	32.12	28.64	35.77	31.78	30.40	29.98	30.61
10	D39	32.44	28.96	36.17	32.09	30.65	30.46	30.96
11	D40	32.31	28.96	36.16	32.19	30.63	30.49	30.96
12	D41	31.88	28.54	35.59	31.68	30.35	29.91	30.49
13	D42	30.53	28.04	34.79	30.99	30.20	29.68	29.70
14	D43	30.06	27.65	34.63	30.79	30.18	29.58	29.55
15	D44	30.41	28.02	34.74	30.91	30.17	29.66	29.57
16	D45	32.20	28.87	35.96	31.94	30.60	30.33	30.75
17	D46	32.29	28.91	36.20	32.18	30.59	30.51	30.82
18	D47	31.94	28.54	35.66	31.70	30.39	29.93	30.48
19	D48	32.12	28.55	35.73	31.75	30.41	29.93	30.54
20	D49	32.01	28.64	35.80	31.76	30.42	30.07	30.53

Table 4. Relationship between the complexity and reconstruction performances.

ID	Dictionary	PSNR	Complexity (10^9)	ID	Dictionary	PSNR	Complexity (10^9)
1	D30	30.31	0.18	11	D40	32.31	0.89
2	D31	31.95	3.10	12	D41	31.88	1.18
3	D32	32.43	2.12	13	D42	30.53	0.19
4	D33	32.14	0.47	14	D43	30.06	0.25
5	D34	31.88	0.53	15	D44	30.41	0.19
6	D35	32.23	3.23	16	D45	32.20	1.54
7	D36	32.39	0.33	17	D46	32.29	1.60
8	D37	30.47	0.24	18	D47	31.94	2.09
9	D38	32.12	2.16	19	D48	32.12	1.44
10	D39	32.44	1.72	20	D49	32.01	1.24

B. On performance evaluation

We evaluate the proposed dictionary training samples-optimized sparse reconstruction-based MR images super-resolution. We repeated the experiments with the Monte-Carlo simulation method. In the experiments, we implemented 1:2 and 1:4 of image super-resolution MR to evaluate the performance of the MR sequence. The MR images are obtained through the down-sampling for performance evaluation. In the experimental procedural parameters, Overlaps is 4, λ=0.1. For the comparison, we implement three MR super-resolution methods including the traditional SR-based MR super-resolution, Bicubic Interpolation (BI), and the proposed optimal selecting training samples-based sparse representation construction of MR image. The performance of the super-resolution methods is measured by PSNR. The results are shown in Table 5. These results show that the proposed method is feasible to improve SR-based MR super-resolution. The results show that sufficient use of the definite MR samples is a crucial issue of improving the MR super-resolution. For joint dictionary learning, training samples will directly affect the quality of the image reconstruction effect of sparse image reconstruction, so the sample selection is one of the most important research problems in dictionary learning.

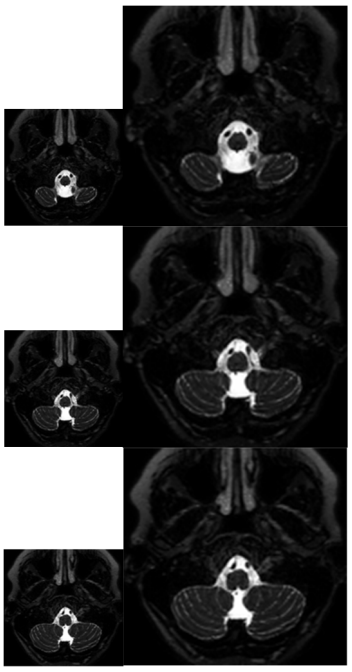

Fig.3. Examples of MR sequence super-resolution.

The traditional training method requires a large number of training samples to ensure the effectiveness of training dictionary blocks, more training samples possess relatively more prior knowledge. The trained dictionary can make the reconstruction of the image closer to the actual, but the sample is rich to ensure effective training samples. The poor quality of the samples not only provides high quality image reconstruction, it may also lower the value of the PSNR super resolution reconstruction. The proposed textural complexity-based image quality representation is feasible to select the optimal training images. The simultaneous training of low-high resolutions dictionaries is to enhance the similarity of sparse representations for sparse reconstruction-based super-resolution MR imaging. Some 1:2 of super-resolution examples are shown in Fig.3.

Other experiments are implemented on the real MR database from Harbin Medical University (HMU). This MR database includes 150 MR images, and we repeated the experiments with the Monte-Carlo simulation method. The PSNR value is to measure the performance of super-resolution. For the comparison, other super-resolution methods, Sparse Representation Reconstruction (SRR), Bicubic Interpolation (BI), and Neighborhood Embedding (NE), are used to compare the performance of the algorithms. The 1:2 and 1:4 of super-resolution rates are selected in the experiments. As results show in Table 6., the proposed algorithm achieves the highest performance. Learning-based super-resolution method is feasible to enhance the performance of image super-resolution.

Table 5. Performance evaluation of 1:2 and 1:4 of MR super-resolution.

	Methods	**1:4 super-resolution**	**1:2 super-resolution**
Skull Base	BI	32.54±1.54	34.65±1.26
	SRR	33.65±1.65	35.56±1.32
	Proposed	33.89±1.56	35.90±1.25
Carotid Arteries	BI	28.65±1.46	30.46 ±1.53
	SRR	29.56±1.56	31.65 ±1.68
	Proposed	30.25±1.44	32.25 ±1.56
Knee	BI	27.48±1.85	30.24±1.88
	SRR	28.56±1.65	31.36±1.86
	Proposed	29.86±1.75	32.56±1.36
Ankle	BI	27.36±1.66	30.52±1.83
	SRR	28.16±1.57	31.56±1.74
	Proposed	28.86±1.59	32.23±1.53
Ankle_pd	BI	27.42±1.58	30.25±1.85
	SRR	28.12±1.45	31.85±1.68
	Proposed	27.42±1.58	32.13±1.62
Aorta	BI	33.85±1.64	35.26±1.53
	SRR	34.12±1.56	36.46±1.56
	Proposed	34.97±1.34	36.96±1.63
Neck	BI	30.89±1.76	32.36±1.65
	SRR	31.35±1.53	33.12±1.76
	Proposed	32.23±1.86	33.86±1.86

Table 6. Performance evaluation on Harbin Medical University.

Methods	**1:2 super-resolution**	**1:4 super-resolution**
BI	30.26±0.76	27.52±0.64
NE	31.15±0.53	28.45±0.51
SRR	32.53±0.56	29.36±0.52
Proposed	32.86±0.65	29.78±0.56

4. CONCLUSION

We propose a framework of dictionary block-optimized sparse reconstruction-based super-resolution MR imaging. The paper aims to overcome the problem that the resolution of MR hardware imaging reaches the limitation of resolution due to the increasing of radiation intensity and time of magnetic exposure. The image quality representation based on complex procedures is presented for training the high-low MR image blocks. Comprehensive evaluations are implemented to test the feasibility and performance of the SR-MR method on the real database. Texture complexity of MR training images is higher, and then the quality of super-resolution is better. The optimal training images are selected for the training dictionary, the samples that are not fitted to the dictionary training of MR images are deleted. The super-resolution performance is improved. The proposed method can be applied to images super-resolution, video super-resolution applications. In the experiments, we use MR images of healthy volunteers to train the dictionary. But the coverage of all potential pathologies is not testified. The proposed algorithm improves the visual quality of MR images, but the performance of recovering the hidden pathology from the lower resolution of image is not testified. The feasibility on recovering the hidden information will be studied in the future work.

ACKNOWLEDGMENT

This work is supported by National Science Foundation of China under Grant No. 61671170, 61371178, Program for New Century Excellent Talents in University under Grant No. NCET-13-0168, Natural Science Foundation of Heilongjiang under Grant No. F2015003, Harbin Science and Technology Innovation Talent Research Special Fund (Youth Talent) under Grant No. 2015RQQXJ088, Guangxi Key Laboratory of Automatic Detecting Technology and Instruments under Grant No. YQ16201, the Open Projects Program of National Laboratory of Pattern Recognition, Fundamental Research Funds for the Central Universities under Grant No. HIT.BRETIII.201206, and Program for Interdisciplinary Basic Research of Science-Engineering-Medicine at the Harbin Institute of Technology.

REFERENCES

[1] Malathi, G., Shanthi, V. (2011). Statistical measurement of ultrasound placenta images complicated by gestational diabetes mellitus using segmentation approach. *Journal of Information Hiding and Multimedia Signal Processing*, 2 (4), 332-343.

[2] Lee, C.F., Chang, W.T. (2010). Recovery of color images by composed associative mining and edge detection. *Journal of Information Hiding and Multimedia Signal Processing*, 1 (4), 310-324.

[3] Kaganami, H.G., Ali, S.K. Zou, B. (2011). Optimal approach for texture analysis and classification based on wavelet transform and neural network. *Journal of Information Hiding and Multimedia Signal Processing*, 2 (1), 33-40.

[4] Hu, W.C., Yang, C.Y., Huang, D.Y., Huang, C.H. (2011). Feature-based face detection against skincolor like backgrounds with varying illumination. *Journal of Information Hiding and Multimedia Signal Processing*, 2 (2), 123-132.

[5] Peng, C.Y., Li, J.W. (2012). Fast sparse representation model for l1-norm minimisation problem. *Electronics Letters*, 48 (3), 162-164.

[6] Chavez-Roman, H., Ponomaryov, V. (2014). Super resolution image generation using wavelet domain interpolation with edge extraction via a sparse representation. *IEEE Geoscience & Remote Sensing Letters*, 11 (10), 1777-1781.

[7] Engan, K., Aase, S.O., Husey, J.H. (1999). Method of optimal directions for frame design. In *IEEE International Conference on Acoustics, Speech and Signal Processing*. IEEE, 5, 2443-2446.

[8] Li, Y., Namburi, P., Yu, Z., Guan, C. (2009). Voxel selection in fMRI data analysis based on sparse representation. *IEEE Transactions on Biomedical Engineering*, 56 (10), 2439-2452.

[9] Xu, D., Huang, Y., Zeng, Z., Xu, X. (2012). Human gait recognition using patch distribution feature and locality-constrained group sparse representation. *IEEE Transactions on Image Processing*, 21 (1), 316-326.

[10] Rubinstein, R., Bruckstein, A.M., Elad, M. (2010). Dictionaries for sparse representation modeling. *Proceedings of the IEEE*, 98 (6), 1045-1057.

[11] Cevher, V., Krause, A. (2011). Greedy dictionary selection for sparse representation. *IEEE Journal of Selected Topics in Signal Processing*, 5 (5), 979-988.

[12] Chen, Y., Nasrabadi, N.M., Trac, D. (2011). Sparse representation for target detection in hyperspectral imagery. *IEEE Journal of Selected Topics in Signal Processing*, 5 (3), 629-640.

[13] Yang, B., Li, S. (2010). Multifocus image fusion and restoration with sparse representation. *IEEE Transactions on Instrumentation and Measurement*, 59 (4), 884-892.

[14] Ogawa, T., Haseyama, M. (2011). Missing image data reconstruction based on adaptive inverse projection via sparse representation. *IEEE Transactions on Multimedia*, 13 (5), 974-992.

[15] Zuo, W., Lin, Z. (2011). A generalized accelerated proximal gradient approach for total-variation-based image restoration. *IEEE Transaction on Image Processing*, 20 (10), 2748-2759.

[16] Kang, L. W., Hsu, C.Y., Chen, H.W., Lu, C.S., Lin, C.Y., Pei, S.C. (2011). Feature-based sparse representation for image similarity assessment. *IEEE Transactions on Multimedia*, 13 (5), 1019-1030.

[17] Gao, S., Tsang, I.W., Chia, L.T. (2010). Kernel sparse representation for image classication and face recognition. *Lecture Notes in Computer Science*, 63 (14), 1-14.

[18] Yang, J., Wright, J., Huang, T. (2010). Image super-resolution via sparse representation. *IEEE Transactions on Image Processing*, 19, 2861-2873.

[19] Zeyde, R., Elad, M., Protter, M. (2012). On single image scale-up using sparse-representations. *Lecture Notes in Computer Science*, 6920, 711-730.

[20] Chavez-Roman, H., Ponomaryov, V. (2014). Super resolution image generation using wavelet domain interpolation with edge extraction via a sparse representation. *IEEE Geoscience & Remote Sensing Letters*, 11 (10), 1777-1781.

[21] Guo, Y., Ruan, S., Landre, J., Constans, J.M. (2011). A sparse representation method for magnetic resonance spectroscopy quantification. *IEEE Transactions on Biomedical Engineering*, 57 (7), 1620-1627.

[22] Wei, Y., Qiu, J., Karimi, H.R., Wang, M. (2014). H-infinity model reduction for continuous-time Markovian jump systems with incomplete statistics of mode information. *International Journal of Systems Science*, 45 (7), 1496-1507.

[23] Wei, Y., Qiu, J., Karimi, H.R., Wang, M. (2014). New results on H-infinity dynamic output feedback control for Markovian jump systems with time-varying delay and defective mode information. *Optimal Control, Applications and Methods*, 35 (6), 656-675.

[24] Wei, Y., Qiu, J., Karimi, H.R., Wang, M. (2015). Quantized H-infinity filtering for continuous-time Markovian jump systems with deficient mode information. *Asian Journal of Control*, 17 (6), 1914-1923.

[25] Yang, J., Wright, J., Huang, T. (2010). Image Super-resolution via sparse representation. *IEEE Transactions on Image Processing*, 19 (11), 2861-2873.

[26] Wang, J., Zhu, S., Gong, Y. (2010). Resolution enhancement based on learning the sparse association of image paths. *Pattern Recognition Letters*, 31 (1), 1-10.

Received March 29, 2017.
Accepted May 26, 2017.